Journal of Solid State Chemistry 257 (2018) 1–8

Contents lists available at ScienceDirect

Journal of Solid State Chemistry

journal homepage: www.elsevier.com/locate/jssc

A neutron diffraction study of the hexagonal Laves phases, $Ho(Co_{0.667}Ga_{0.333})_2$ and $Er(Co_{0.667}Ga_{0.333})_2$: Co/Ga site preferences and magnetic structure

Fang Yuan[a], John E. Greedan[a], Chad Boyer[b], Yurij Mozharivskyj[a,*]

[a] Department of Chemistry and Chemical Biology, Brockhouse Institute of Materials Research, McMaster University, 1280 Main Street West, Hamilton, Ontario, Canada L8S 4M1

[b] Canadian Neutron Beam Centre, Canadian Nuclear Laboratories, Chalk River, Canada K0J 1J0

ARTICLE INFO

Keywords:
hexagonal Laves Hexagonal Laves phases
Neutron powder diffraction
Crystal structure
Magnetic properties
Small angle neutron scattering

ABSTRACT

$RE(Co_{0.667}Ga_{0.333})_2$ (*RE* = Ho, Er) were characterized by neutron powder diffraction (NPD). Rietveld refinement of the NPD data at 280 K confirms the hexagonal $MgZn_2$-type structure ($P6_3/mmc$), in accordance with the previous XRD results. Co/Ga occupancies on the 2*a* and 6*h* sites were refined to be 0.46/0.54(2) and 0.74/0.26(2), respectively, indicating a preference of Ga for the 2*a* site and of Co for the 6*h* site. Both materials are ferromagnetic, $\boldsymbol{k}$ = (000), with measureable moments only on the *RE* sites. The magnetic (Shubnikov) space group is $P6_3/mm'c'$ for the Er phase. Co moments refined to values of 0.1–0.3 μ_B and are effectively zero within 3σ. The Er moment, 6.07(8) μ_B at 3.5 K is parallel to the *c* axis and this orientation persists up to T_C = 18.5 K, while the Ho moment has components along both the *a* and *c* axes with a total moment of 6.3(1) μ_B at 3.5 K. Both moments are much reduced from the free ion values, 9 μ_B (Er) and 10 μ_B (Ho), which is attributed to crystal field effects. In addition, the Ho moment angle with the *c* axis is strongly temperature dependent, being roughly constant, ~ 24(6)° from *T* = 29 K to ~25 K, then increasing with decreasing temperature to 44(1)° at 3.5 K. Magnetic small angle neutron scattering (MSANS) was observed over a *Q*-range from 0.14 $Å^{-1}$ to 0.50 $Å^{-1}$ in both samples. The integrated MSANS of the Er phase peaks near T_C, then decreases monotonically with decreasing temperature, behavior typical for a simple ferromagnet. On the other hand, the integrated MSANS for the Ho phase exhibits a weak peak around T_C = 31 K, followed by a plateau to 25 K and a strong increase with decreasing temperatures, which tracks the evolution of the Ho moment angle with the *c* axis.

1. Introduction

The $RECo_2$ (*RE* = rare earth) compounds have been well studied [1–5]. While all $RECo_2$ adopt the same cubic $MgCu_2$-type structure, their magnetic properties are quite different with regard to the rare-earth element. A novel type of short-range order, an exchange enhanced paramagnetism, has been identified in nonmagnetic $ScCo_2$, YCo_2, and $LuCo_2$, while a long-range magnetic order is found in $RECo_2$ with magnetic rare-earth elements [6]. In the latter case, the Co sublattice is driven into a ferromagnetic state by an *f-d* exchange field and the moment in the ordered state is between 0.8 and 1 μ_B. The light $RECo_2$ phases are ferromagnetic with the Co and *RE* sublattice coupling parallel. On the other hand, the heavy $RECo_2$ phases are best characterized as ferrimagnetic wherein the *RE* moments couple anti-parallel to the Co moments [7]. The magnetic phase transition for at least some members of the series, *RE* = Dy, Ho and Er, is apparently first order and thus, these have been evaluated recently as potential magnetocaloric materials [3,8]. Therefore, the studies on the heavy $RECo_2$-based phases have been attracting increasing attention.

While the $RECo_2$ materials adopt the cubic ($Fd\bar{3}\ m$) Laves phase structure, substitution of Ga for Co induces the formation of the hexagonal ($P6_3/mmc$) $MgZn_2$-type structure in the $RE(Co_{0.667}Ga_{0.333})_2$ series [9]. All studied $RE(Co_{0.667}Ga_{0.333})_2$ (*RE* = Gd, Tb, Dy, Ho and Er) phases show a long-range order but the Curie temperatures are reduced by a factor of ~ 2.5 from the parent $RECo_2$ phases [3,9] (Fig. 1). Apparent ferromagnetic behavior is observed for *RE* = Gd, Tb and Dy, whose Weiss temperature/Curie temperature ratios are near unity, which is typical for ferromagnets. Also, the effective magnetic moments, μ_{eff} were equal to the *RE* only values, suggesting zero contribution from the Co/Ga sublattice in the paramagnetic region. Exceptions to this trend occur for *RE* = Ho and Er, whose Weiss temperature/Curie temperature ratios are 0.66 and −0.65, respectively

* Corresponding author.
E-mail address: mozhar@mcmaster.ca (Y. Mozharivskyj).

http://dx.doi.org/10.1016/j.jssc.2017.09.019
Received 19 July 2017; Received in revised form 13 September 2017; Accepted 17 September 2017
Available online 19 September 2017
0022-4596/

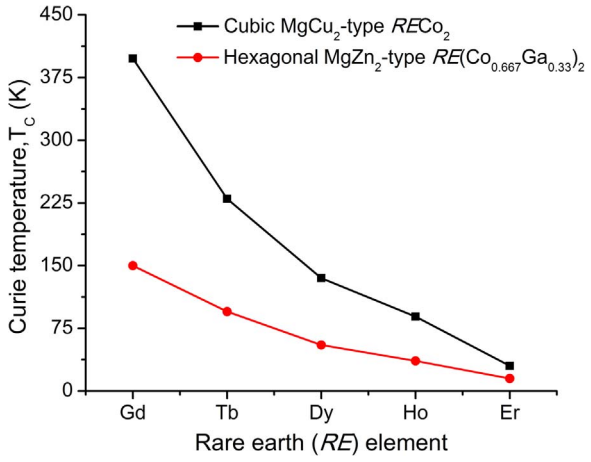

Fig. 1. The Curie temperature of cubic $RECo_2$ and hexagonal $RE(Co_{0.667}Ga_{0.333})_2$ (RE = Gd, Tb, Dy, Ho, and Er).

(the Weiss temperature is negative for Er). As well, μ_{eff} values exceeded those for the RE ions only, suggesting a non-zero Co/Ga contribution and the possibility of a moment on that sublattice.

Finally, there are two Co/Ga sites in the $MgZn_2$-type structure, and the Co/Ga occupancies could not be refined due to their similar X-ray atomic scattering factors. On the other hand, the neutron scattering lengths, b, are significantly different for Co (b = 2.49 fm) and Ga (b = 7.29 fm), and thus they are readily distinguished by neutron diffraction [10]. In this work, neutron powder diffraction (NPD) was used to determine the magnetic structures and the magnetic moments at each site of the hexagonal $MgZn_2$-type $RE(Co_{0.667}Ga_{0.333})_2$ (RE = Ho, Er) phases and the Co/Ga occupancies.

2. Experimental section

2.1. Synthesis

The starting materials of $RE(Co_{0.667}Ga_{0.333})_2$ (RE = Ho, and Er) phases are RE (99.9 wt%, distilled grade, Metal Rare Earth Limited, China), Co (99.98 wt%, Alfa Aesar), and Ga (99.999 wt%, Alfa Aesar) pieces. The $RE(Co_{0.667}Ga_{0.333})_2$ alloys with a total mass of ~3 g were arc-melted 3 times to ensure homogeneity. During re-melting process, the samples were turned over as fast as possible to prevent sample cracking during cooling. The cast $RE(Co_{0.667}Ga_{0.333})_2$ (RE = Ho, and Er) alloys were wrapped in Ta foil, sealed in evacuated silica tubes, heated to 1000 °C at 100 °C/hour in the box furnaces and annealed for 72 h before being quenched in cold water.

2.2. Neutron powder diffraction

Neutron powder diffraction was performed on the C2 diffractometer at the Canadian Neutron Beam Centre at Chalk River, Ontario. The samples of ~ 2 g were mounted on a cylindrical vanadium container with a top-loading closed-cycle refrigerator. The data were collected using the neutron beams with a wavelength of 2.369(1) Å at 3.5 K, 280 K, and other temperatures between 3.5 K and Curie temperature (T_C) for 2θ = 3.0–83.1°, and with a wavelength of 1.327(1) Å at 3.5 K and 280 K for 2θ = 36.9–117.0°. The 2θ step size was 0.1° for all the data collection. The FullProf program [11] was used to refine the crystal and magnetic structures.

2.3. Electronic band structure calculations

To study the band structure of hexagonal $MgZn_2$-type $Er(Co_{0.667}Ga_{0.333})_2$ phase and understand the absence of Co moments, tight-binding, linear-muffin tin orbital calculations with the atomic sphere approximation [12] (TB-LMTO-ASA) as implemented in the Stuttgart program [13] were performed. The lattice parameters and atomic coordinates were taken from the previous single crystal X-ray refinements [9]. All 4f electrons were treated as core electrons. Exchange and correlation were treated by the local density approximation (LDA) [14]. A scalar relativistic approximation [15] was used to account for all relativistic effects except spin-orbit coupling. According to the atomic sphere approximation (ASA), overlapping Wigner-Seitz (WS) cells were constructed with radii making the overlapping potential to be the best approximation to the full potential. To satisfy the overlap criteria of the TB-LMTO-ASA model, space-filling empty spheres were included in the unit cell by the automatic sphere generation [16]. The basis set included 6s, 6p and 5d orbitals for Er, 4s, 4p, 3d, orbitals for Co, 4s, 4p, and 4d orbitals for Ga.

3. Results and discussion

3.1. Crystal structure

Rietveld refinement of the neutron powder diffraction data of $RE(Co_{0.667}Ga_{0.333})_2$ (RE = Ho, and Er) are consistent with the $MgZn_2$-type structure, conforming the previous X-ray diffraction results [9] (Table 1). There are three crystallographic sites in the hexagonal $MgZn_2$-type structure: 2a, 4f and 6h. The RE atoms occupy the 4f site, while Co/Ga are distributed over the 2a and 6h sites but their occupancies could not be previously refined due to their similar X-ray atomic scattering factors (Z_{Co} = 27 and Z_{Ga} = 31). However, as already noted, there is significant neutron scattering length contrast [10]. Herein, the Co/Ga occupancies were refined employing the neutron powder diffraction with a wavelength of 1.327(1) Å at 280 K.

Due to strong correlations, the site occupancy and displacement parameter were not refined simultaneously. The occupancies of RE atom sites were fixed at 100%, which was confirmed by the single crystal X-ray diffraction in our previous work [9]. Displacement parameters for the three sites were varied for a set of fixed occupancies for the 2a site, which spanned the full range of possibilities. The results for both materials in terms of the Ga fraction, x, of the 2a site are shown in Fig. 2. The χ^2 value is minimized when the isotropic displacement parameters on the 2a and 6h sites are roughly equal. At the point of intersection, x is about 13/24, i.e. Ga occupies 13/24 (0.54) of the 2a sites, while the remaining 11/24 (0.46) fraction is taken by Co. Because the total Co/Ga ratio is 2, the Co and Ga occupancies on 6h sites are 53/72 (0.74) and 19/72 (0.26), respectively (Table 2). Note that the results are essentially the same for Ho and Er

Table 1
Unit cell parameters of the $MgZn_2$-type $RE(Co_{0.667}Ga_{0.333})_2$ phases (RE = Ho and Er, XRD and NPD were collected at room temperature and 280 K, respectively).

Sample	Method	λ/Å	Structure type	a/Å	c/Å	R_P
$Ho(Co_{0.667}Ga_{0.333})_2$	XRD	1.5406	$MgZn_2$-type	5.2064(1)	8.4228(1)	6.22
$Ho(Co_{0.667}Ga_{0.333})_2$	NPD	1.327 (1)	$MgZn_2$-type	5.2027(3)	8.4248(7)	3.89
$Ho(Co_{0.667}Ga_{0.333})_2$	NPD	2.369 (1)	$MgZn_2$-type	5.2048(6)	8.429(1)	3.52
$Er(Co_{0.667}Ga_{0.333})_2$	XRD	1.5406	$MgZn_2$-type	5.1851(1)	8.4115(1)	5.53
$Er(Co_{0.667}Ga_{0.333})_2$	NPD	1.327 (1)	$MgZn_2$-type	5.1853(4)	8.4159(9)	3.76
$Er(Co_{0.667}Ga_{0.333})_2$	NPD	2.369 (1)	$MgZn_2$-type	5.1871(6)	8.418(1)	4.46

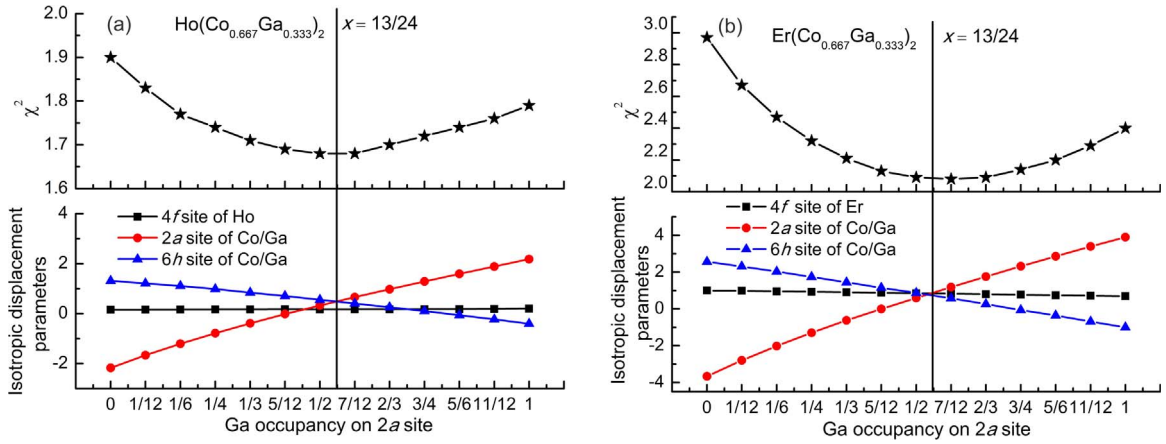

Fig. 2. Refinement of the Co/Ga occupancies based on χ^2: (a) $Ho(Co_{0.667}Ga_{0.333})_2$, (b) $Er(Co_{0.667}Ga_{0.333})_2$.

and that Ga prefers the 2*a* site and Co the 6*h* site.

Although Ga and Al belong to the same group and have nearly identical atomic size (r_{Al} = 1.25 Å and r_{Ga} = 1.26 Å) [17], the site occupancy in the pseudo-binary $RECo_2$-$REGa_2$ systems is different from that in the pseudo-binary $RECo_2$-$REAl_2$ systems. $Er(Co_{1-x}Al_x)_2$ pseudo-binary phases with the $MgZn_2$-type structure have a random distribution of Co and Al on the 2*a* and 6*h* sites at lower Al concentration, i.e. $x \leq 0.5$. When $x > 0.5$, Co seems to occupy 2*a* sites exclusively, and Al and Co coexist on 6*h* site [18]. While x = 0.333 in the $RE(Co_{1-x}Ga_x)_2$ (*RE* = Ho, and Er) phases, Ga and Co exhibit obvious preferences for the 2*a* and 6*h* sites, respectively.

3.2. Magnetic structures

Selected neutron diffraction data are shown in Fig. 3**a and b** for $RE(Co_{0.667}Ga_{0.333})_2$ (*RE* = Er, and Ho) at the base temperature of the cryostat, 3.5 K, and at temperatures just above the estimated Curie temperatures. There are at least two features to note. First, the 3.5 K data contain several new reflections of significant intensity, indicating that they are magnetic in origin. Secondly, there is very strong scattering below 10° which can be assigned as magnetic small angle neutron scattering (MSANS). As will be shown later, no such low angle scattering exists in the 280 K data.

In Fig. 3**c** and **d**, differences between the intensities at 3.5 K and higher temperatures isolate the magnetic reflections. Some of the low angle reflections, which provide information regarding the direction of the magnetic moments, are indexed. For the Ho phase there are three such peaks, (100), (002) and (101), while in the Er case, the (002) is absent. Clearly, the ordering wave vector is $\boldsymbol{k}$ = (0, 0, 0) for both. Fig. 4 shows the simulation of NPD patterns for $Ho(Co_{0.667}Ga_{0.333})_2$ with an ordered moment of 8 μ_B and a ferromagnetic model, F_z or $F_{x,y}$. As verified by the simulations in Fig. 4, the $Er(Co_{0.667}Ga_{0.333})_2$ moment must be parallel to the *c* axis, while the $Ho(Co_{0.667}Ga_{0.333})_2$ moment likely has components in both the *ab* plane and along the *c* axis. The agreement between the observed and simulated NPD patterns with ferromagnetic models strongly suggest ferromagnetic ground states for $RE(Co_{0.667}Ga_{0.333})_2$ (*RE* = Er and Ho).

3.2.1. $Er(Co_{0.667}Ga_{0.333})_2$

The magnetic structure of $Er(Co_{0.667}Ga_{0.333})_2$ was refined at 3.5 K using the data from both wavelengths. For these refinements the Co/Ga site occupations from the 280 K data were assumed and the Er (*z*) and Co/Ga (*x*, *y*) positions were refined along with an overall atomic displacement parameter and, of course, the lattice constants. The positional parameters did not change significantly from the 280 K refinement. Initially, a F_z model for the Er moments with no contribution from the Co/Ga lattice was refined. The results are shown in Fig. 5 and Table 3. The Er moment is indeed along the *c* axis and its refined value is 6.07(8) μ_B. This is significantly reduced from the free ion value of $g_J J$ = 9 μ_B expected for Er^{3+}, indicating that crystal field effects are important in $Er(Co_{0.667}Ga_{0.333})_2$. A model with moments on both the 2*a* and 6*h* sites and antiparallel to the Er moment on the 4*f* site was also refined. There was no change in the agreement indices, χ^2 or R_{mag}, and the moments on the Co/Ga sites were refined to 0.12(6) μ_B, which is in fact zero within 2σ. The Er moment was reduced to 5.8(1) μ_B, which is within 3σ from the value obtained by excluding any Co contribution. The conclusion is that there is no compelling evidence for a moment on the Co/Ga sites in this material. This is in contrast to the situation for $ErCo_2$, where the Co moment is ~ 1 μ_B [19], a factor of ~ 10 larger than refined for $Er(Co_{0.667}Ga_{0.333})_2$.

NPD patterns were also obtained using the λ = 2.369(1) Å wavelength for several temperatures and the Er moment was refined within the F_z model. The results are shown in Fig. 6**b** along with the observed intensities for the (100) and (101) magnetic reflections of Fig. 6**a**. Note the very gradual decrease in the intensities (Fig. 6**a**) and ordered moment (Fig. 6**b**) up to T_C ~ 18.5 K, which is 23% higher than T_C of 15 K estimated from the magnetization data. There are uncertainties in the determination of T_C from Fig. 6. First, both "magnetic" reflections, (100) and (101), have small structural components, that for the latter is somewhat greater than for the former.

Table 2
Atomic coordinates and isotropic displacement parameters (B_{eq}) for annealed $RE(Co_{0.667}Ga_{0.333})_2$ (*RE* = Er, and Ho) at 280 K.

Atom	Site	Occupancy	x/ *a*	y/ *b*	z/ *c*	B_{eq} (Å^2)	R_P
Ho ($Co_{0.667}Ga_{0.333}$)$_2$							
Ho1	4*f*	1	1/3	2/3	0.0631(4)	0.17(9)	3.89
Co1/Ga11	2*a*	0.46/0.54(2)	0	0	0	0.5(1)	
Co2/Ga22	6*h*	0.74/0.26(2)	0.830(2)	0.660(3)	1/4	0.5(1)	
Er($Co_{0.667}Ga_{0.333}$)$_2$							
Er1	4*f*	1	1/3	2/3	0.0626(1)	0.8(1)	3.76
Co1/Ga11	2*a*	0.46/0.54(2)	0	0	0	0.9(2)	
Co2/Ga22	6*h*	0.74/0.26(2)	0.828(2)	0.657(5)	1/4	0.7(1)	

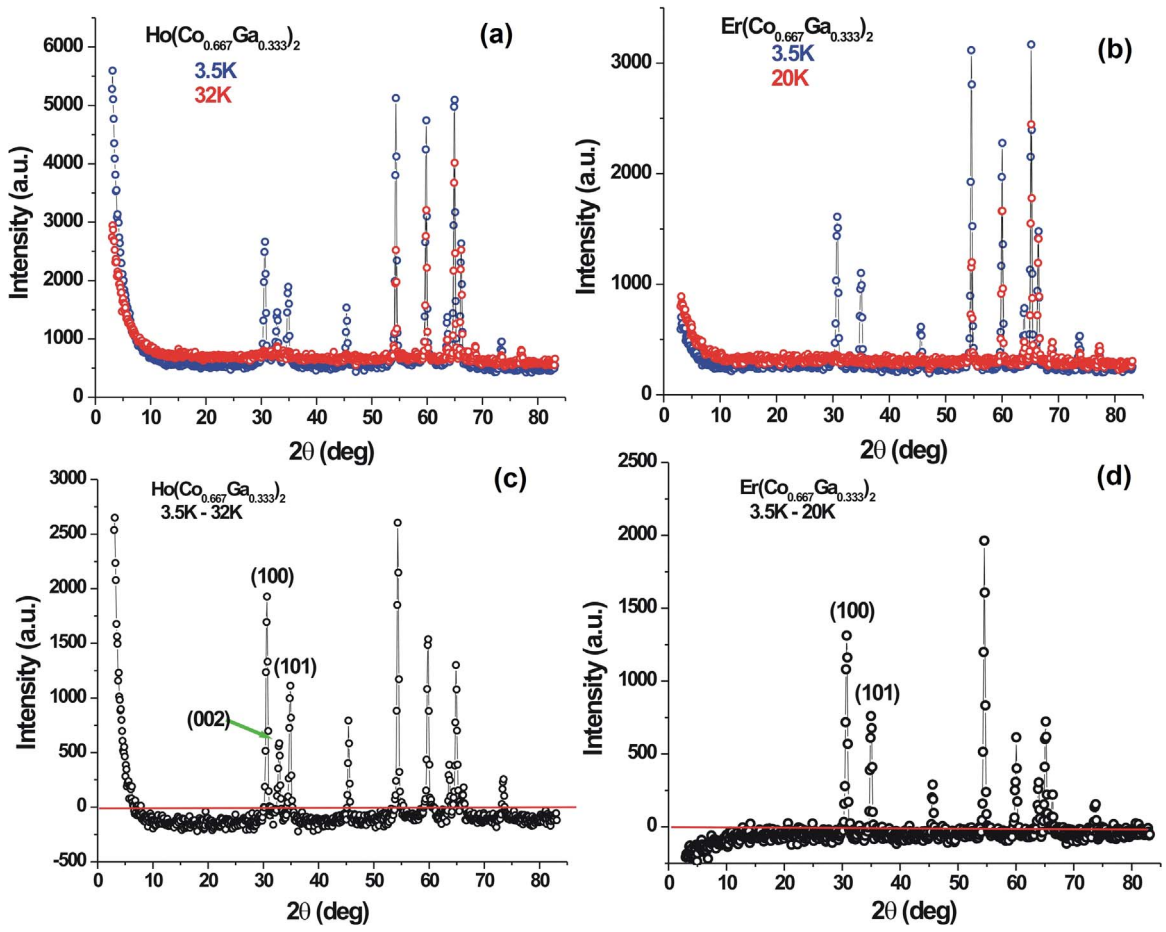

Fig. 3. (a) Comparison of neutron diffraction (ND) patterns for $Ho(Co_{0.667}Ga_{0.333})_2$ at 32 K (red) and 3.5 K (blue). **(b)** Comparison of ND patterns for $Er(Co_{0.667}Ga_{0.333})_2$ at 20 K (red) and 3.5 K (blue). **(c)** Difference ND pattern (3.5–32 K) with some low angle peaks indexed for $Ho(Co_{0.667}Ga_{0.333})_2$. **(d)** Difference ND pattern (3.5–20 K) with some low angle peaks indexed for $Er(Co_{0.667}Ga_{0.333})_2$. In all cases λ = 2.369(1) Å. (For interpretation of the references to color in this figure legend, the reader is referred to the web version of this article).

Secondly, the magnetic component builds rather slowly with decreasing temperature. The (100) reflection is not detectable above 18 K while the (101) reflection retains a small but constant value. This is best seen from the inset, Fig. 6**a**, which shows the $(\text{Intensity})^{1/2}$ for both reflections. While a small Er moment is refined at 19 K, this may result from difficulties in accounting for the weak structural contributions to these reflections. For example R_{mag} at 19 K is 47% while it is 2.5% at 3.5 K and 16% at 17 K. Thus, an assignment of T_C = 18.5 K appears to be the best choice, given the quality of the refinement at 19 K. Finally, the very gradual temperature variation of the moment suggests a large value for the critical exponent, β, in $M(Er)/M(Er)_{sat} = \{[T_C - T]/ T_C\}^{\beta}$. Although there are insufficient data to determine β properly, an estimate was made using data from 18 to 13 K. The fit yielded β = 0.51(2) with T_C = 18.5 K, which is consistent with the mean field theory (MFT) value of 1/2 (Fig. 7). The fact that the MFT appears to hold is in turn consistent with an exchange coupling mechanism such as RKKY that extends over several sets of neighbors in direct space [20–22].

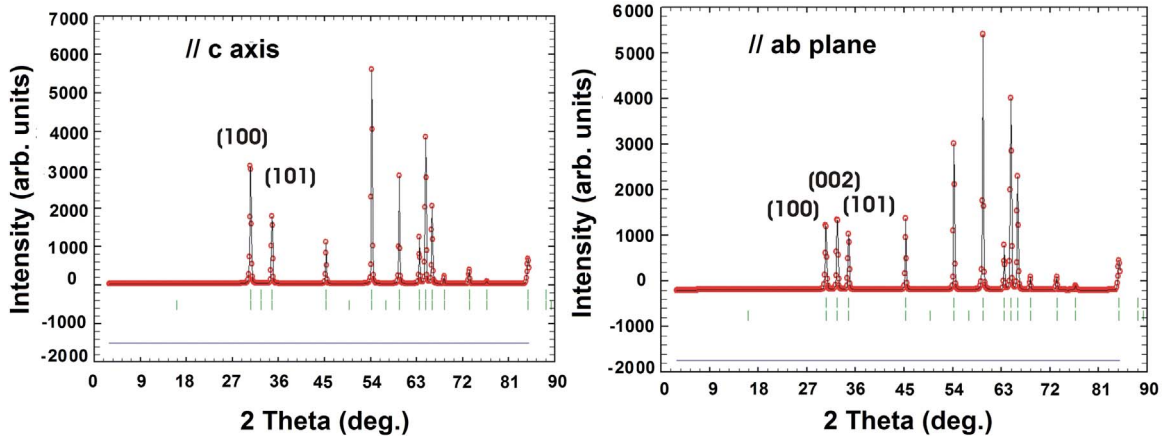

Fig. 4. Simulation of powder neutron diffractions patterns for $Ho(Co_{0.667}Ga_{0.333})_2$ with an ordered moment of 8 μ_B and a ferromagnetic model, F_z or $F_{x,y}$. **(left)** M_{Ho} // c axis, and **(right)** $M_{Ho} \perp c$ axis.

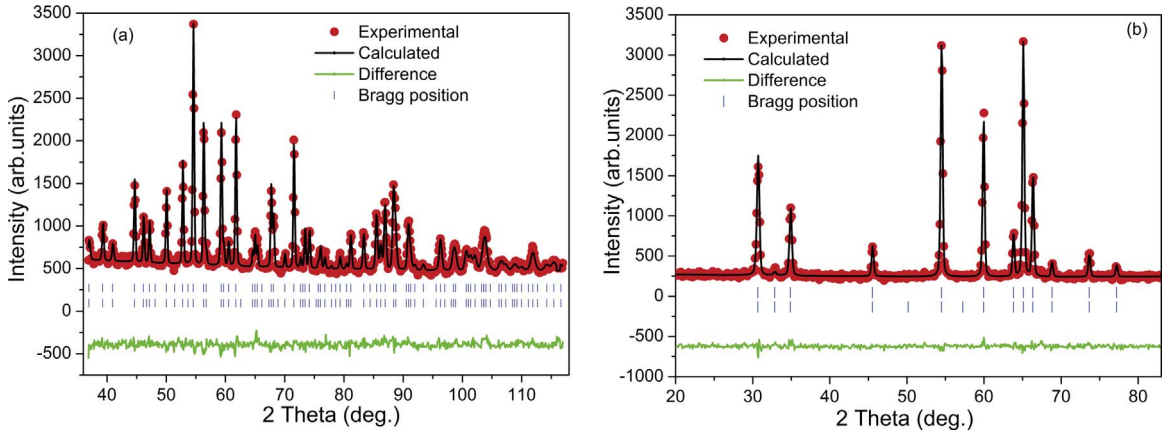

Fig. 5. Rietveld refinement of NPD data for $Er(Co_{0.667}Ga_{0.333})_2$ at 3.5 K with a F_z model for the Er moments and zero moment on the Co/Ga sites. (a) λ = 1.327(1) Å. (b) λ = 2.369(1) Å. The upper and lower sets of tic marks refer to the crystal and magnetic contributions, respectively. Details are given in Table 3.

Table 3
Results of the magnetic structure refinement at 3.5 K for $Er(Co_{0.667}Ga_{0.333})_2$.

Parameter	Value
λ (Å)	2.369(1)
a (Å)	5.1756(2)
c (Å)	8.3847(4)
Er Mom. (μ_B)	6.07(8)
R_{wp}, R_{mag}, χ^2	6.15, 2.54, 1.28

3.2.2. $Ho(Co_{0.667}Ga_{0.333})_2$

Fig. 8 shows the refinement of neutron diffraction pattern for $Ho(Co_{0.667}Ga_{0.333})_2$ at 3.5 K using the data from both wavelengths and the results are listed in Table 4. The initial model involved components of the Ho moment in the *ab* plane and along the *c* axis, i.e. an $F_{x,z}$ configuration. The Ho moment components were refined as M_x = 4.4(1) μ_B and M_z = 4.6(1) μ_B yielding a total Ho moment of 6.3(1) μ_B for λ = 2.369(1) Å. Thus, the Ho moment is tilted 44(1)° from the *c* axis. As with the Er material, inclusion of moments on the Co/Ga sites did not improve the agreement indices and the Co moments refined to 0.28(12) μ_B, i.e. ~ 0 within 3σ and there was no change in the Ho moment, 6.3(1) μ_B. The Ho moment is much reduced from the free ion value of 10 μ_B due to the quenching effects of the crystal field, similar to the case for Er.

The temperature variation of the intensities (*I*) of the magnetic reflections (100), (002) and (101), the refined magnetic components, M_x and M_z, and the total Ho moment, M_T, along with its angle with respect to the *c* axis are all displayed in Fig. 9. Note first in Fig. 9**a**,

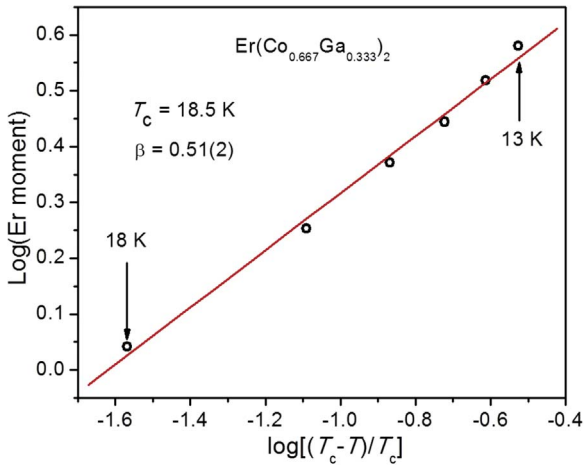

Fig. 7. The relationship between $\log[(T_C - T)/T_C]$ and log(Er moment), where β is the critical exponent and equals the slop of the integrated line (red). (For interpretation of the references to color in this figure legend, the reader is referred to the web version of this article).

from the temperature dependence of the nearly pure magnetic (100) and (101) peaks, that the apparent T_C is 31 K, 14% smaller than T_C of 36 K, estimated from the magnetization data. The (002) reflection has a clear structural component and *I*(002) does not appear to change within error between 25 and 40 K, but increases sharply below 25 K. As the magnetic component of (002) tracks the bending of the total Ho moment away from the *c* axis, it is clear that M_T subtends at least a

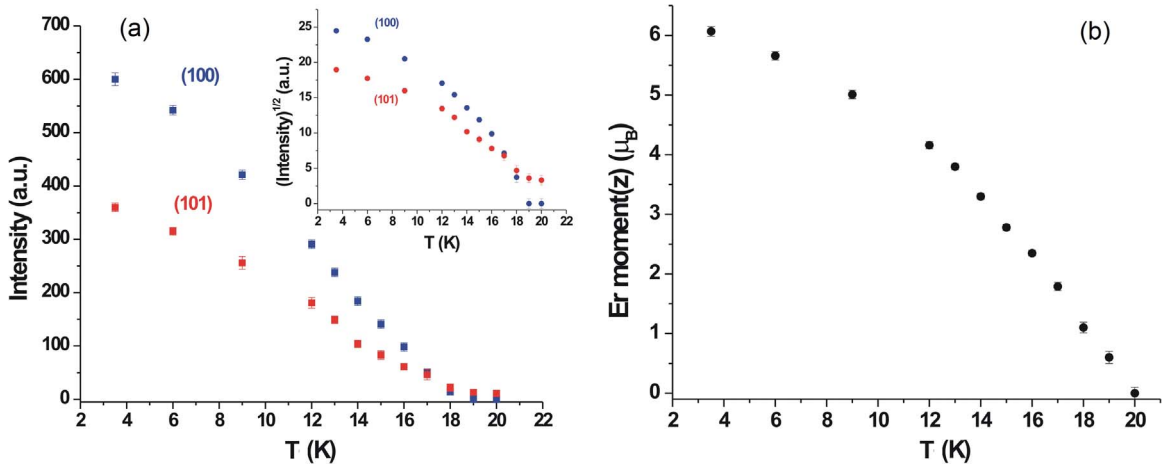

Fig. 6. (a) The temperature variation of the intensities of the (100) and (101) magnetic reflections and the $(intensity)^{1/2}$ (inset). **(b)** The refined Er moment for $Er(Co_{0.667}Ga_{0.333})_2$.

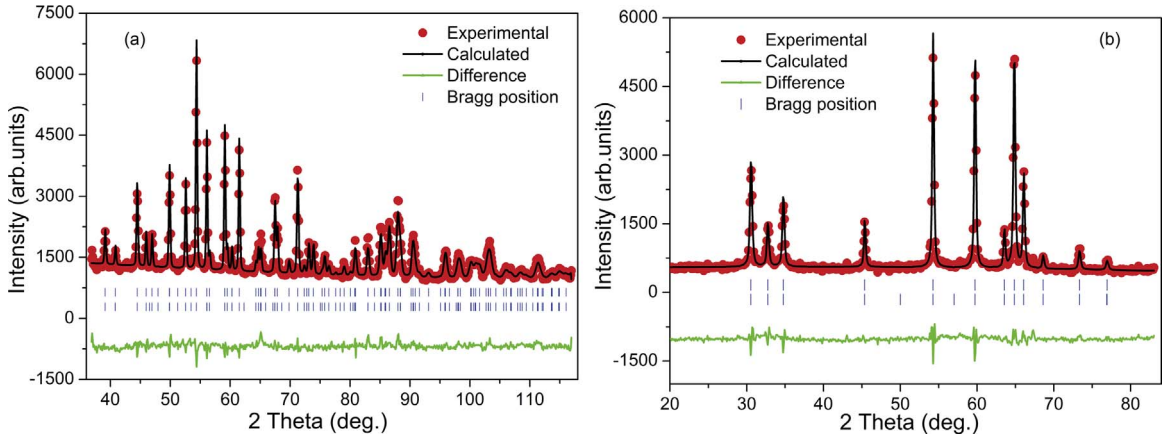

Fig. 8. Rietveld refinement of NPD data for $Ho(Co_{0.667}Ga_{0.333})_2$ at 3.5 K with a $F_{x,z}$ model for the Ho moments and zero moment on the Co/Ga sites. (a) λ = 1.327(1) Å. (b) λ = 2.369(1) Å. The upper and lower set of tic marks indicate the crystal and magnetic structural contributions. Details are given in Table 4.

Table 4
Results of the magnetic structure refinement at 3.5 K for $Ho(Co_{0.667}Ga_{0.333})_2$.

Parameter	Value
λ (Å)	2.369(1)
a (Å)	5.1950(3)
c (Å)	8.4085(6)
M_x, M_z (μ_B)	4.4(1), 4.6(1)
$M_T M_T$ (μ_B)	6.3(1)
R_{wp}, R_{mag}, χ^2	4.94, 7.69, 3.71

constant angle to the c axis from 29 to 25 K, but tilts significantly away during further cooling to 3.5 K. This is reflected in the behavior of the refined components, M_x and M_z (Fig. 9**b**), and the inset shows the temperature variation of the tilt angle, which reaches 44(1)° at 3.5 K as mentioned previously. The value of the tilt angle = $\tan^{-1}(M_x/M_z)$. As can be seen from Fig. 9**b**, the errors on M_x are quite large just below T_C = 31 K. As M_x is largely determined by the relative intensities of I(002) with respect to I(100) and I(101), there may again be difficulties in separating the structural and magnetic contributions associated with (002) during the refinement, thus the large uncertainties in the angle just below T_C.

However, reasonable uncertainties are reached by 25–27 K and it is fair to conclude that the data are consistent with a tilt angle of ~ 24(4)°, which remains constant from 25 K to near T_C. This feature is important in the interpretation of the MSANS data to be discussed in the next section, however, given the issues addressed above, the actual angle is best determined from magnetization measurements on a single crystal. Finally, the difference in magnetic anisotropy between Ho^{3+} and Er^{3+} in this axial crystal system is consistent with observations in other axial materials, for example in the $RECo_5$ series, $P6/mmm$; $ErCo_5$ has an easy c axis anisotropy while for $HoCo_5$ the Ho moment is 50° from the c axis at 4.2 K [23,24].

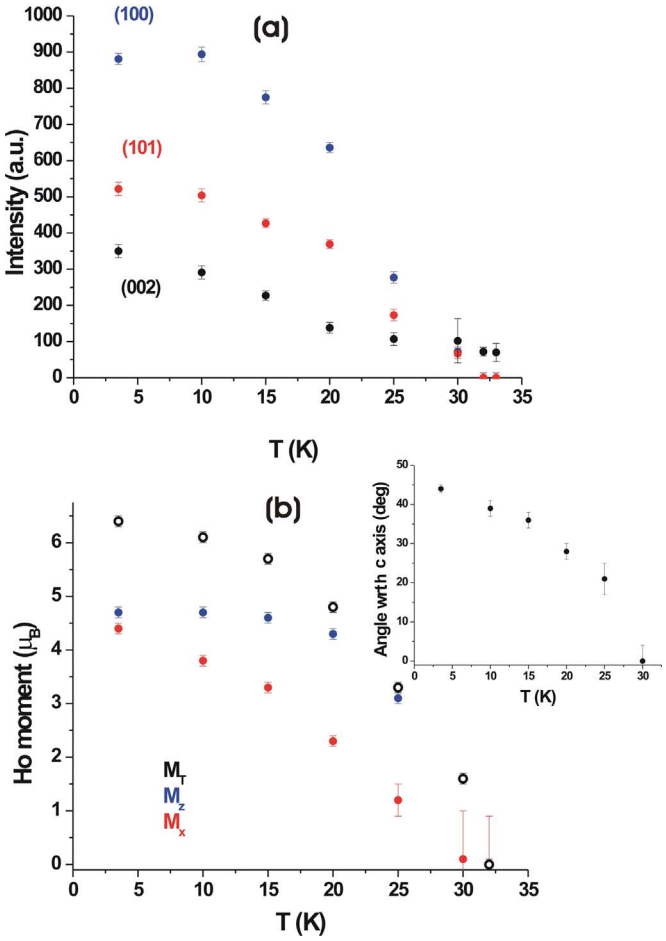

Fig. 9. (a) The temperature variation of the intensities of the (100), (002) and (101) magnetic reflections. **(b)** The refined Ho_x (M_x), Ho_z (M_z) and Ho_{total} (M_T) moments and (inset) the angle made by the Ho moment with respect to the c axis for $Ho(Co_{0.667}Ga_{0.333})_2$.

3.3. Magnetic small angle neutron scattering (MSANS)

Somewhat by accident, MSANS data are also available for both materials (Fig. 3). Normally, MSANS is seen only at very small $Q(2\theta)$ values, where $Q = 4/\lambda\sin\theta$, but the ordered moments on Ho and Er are so large that it can be seen easily in our data, which extend to Q = 0.14 $Å^{-1}$. MSANS is a feature of ferromagnets as there is a very strong peak in the magnetic scattering at $Q(2\theta)$ = 0. A detailed view is provided in Fig. 10 for both materials. Note that the scattering at 280 K is flat in this Q range, which confirms the magnetic origin of the signals near T_C for both materials. Note a surprising feature of the data, namely, that for the $Ho(Co_{0.667}Ga_{0.333})_2$ phase, the MSANS signal increases with decreasing temperature, opposite to the case for Er material. The counting time for data collection of $Ho(Co_{0.667}Ga_{0.333})_2$ and $Er(Co_{0.667}Ga_{0.333})_2$ phase is 3.5 and 4 h respectively, and 1.4 g versus 2.1 g with regard to weight. If the data are scaled to the counting times and weight actually used, the MSANS signal for the former is significantly greater than for the latter.

The magnetic component of the MSANS signal at low temperatures is acquired by subtraction of the 280 K contribution and integration over the Q range (0.14 $Å^{-1} < Q < 0.50$ $Å^{-1}$). The temperature depen-

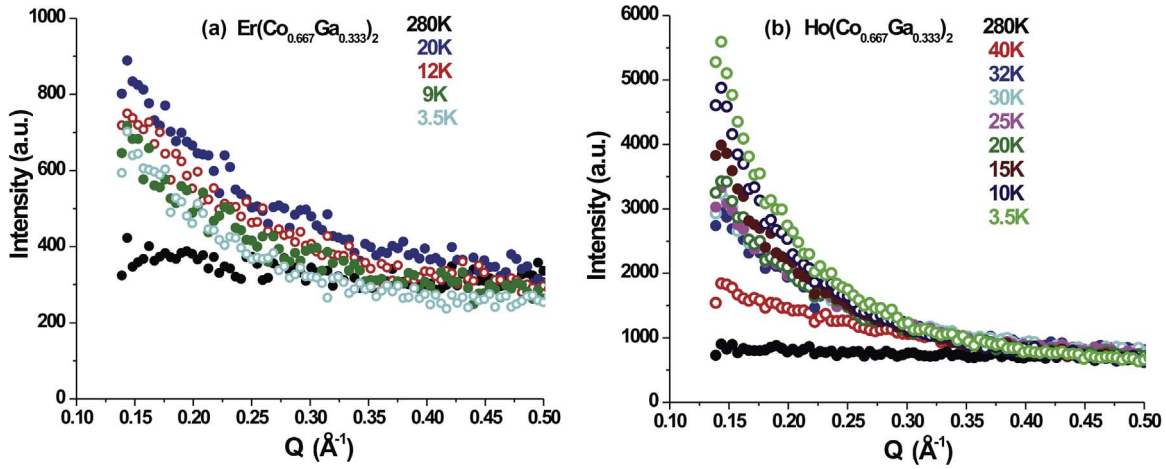

Fig. 10. MSANS data at selected temperatures for (a) $Er(Co_{0.667}Ga_{0.333})_2$ and (b) $Ho(Co_{0.667}Ga_{0.333})_2$. The data are not scaled to the counting times actually used.

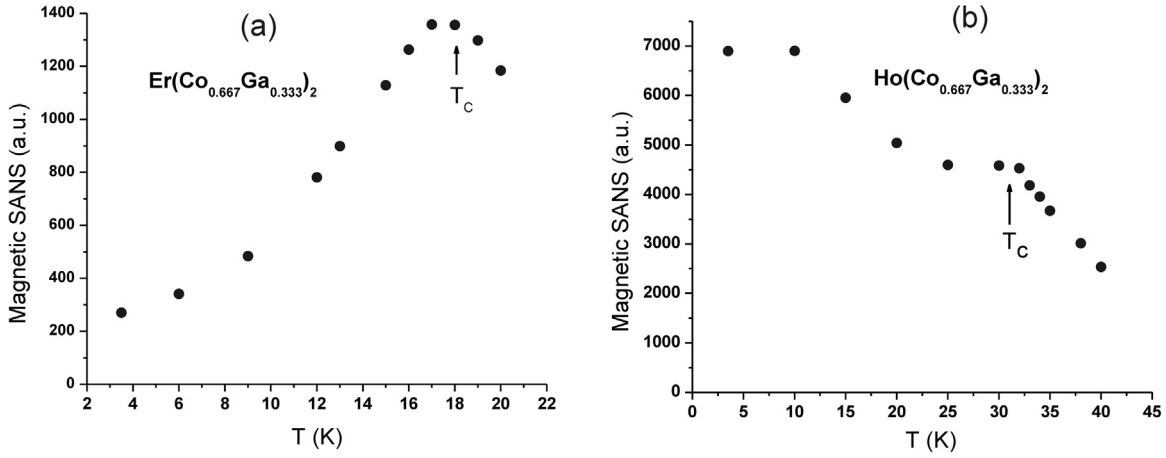

Fig. 11. The temperature dependence of the integrated MSANS data over the range ($0.14\ Å^{-1} < Q < 0.50\ Å^{-1}$) for $Er(Co_{0.667}Ga_{0.333})_2$ **(a)** and $Ho(Co_{0.667}Ga_{0.333})_2$ **(b)**. T_C for both materials is indicated.

dence of the MSANS obtained in this manner is displayed in Fig. 11. The very different behavior of the MSANS component for the two materials is now clearly evident.

The results for $Er(Co_{0.667}Ga_{0.333})_2$ (Fig. 11**a**) are those expected for a simple ferromagnet, for which there are no changes in magnetic structure; MSANS peaks near T_C and then gradually decrease as the ferromagnetic clusters grow in size and pass out of the MSANS window. This is consistent with the strong *c* axis anisotropy for the $Er(Co_{0.667}Ga_{0.333})_2$ phase, which does not change with decreasing temperature. On the other hand, the behavior of the Ho MSANS (Fig. 11**b**) is quite remarkable, showing a weak peak at T_C, followed by a plateau and then by a strong increase leading to another plateau below 10 K. This profile tracks roughly the variation of the Ho moment angle with respect to the *c* axis, Fig. 9**b**, and suggests an explanation for the anomalous behavior, i.e. the magnetic structure just below T_C to ~ 25 K involves a constant Ho tilt angle, giving rise to the MSANS plateau, but below 25 K the angle changes continuously during cooling inducing an increasing MSANS signal.

3.4. The absence of Co magnetic moments

As already mentioned, the Co moments refined to very small values, 0.1–0.2 μ_B which are in fact essentially zero to within 2–3σ. This can be taken as an effective absence of a moment on the Co sites in the $RE(Co_{0.667}Ga_{0.333})_2$ phases studied here. This contrasts with the case of the cubic Laves $RECo_2$ phases, where Co magnetic moment was refined to be ca. 1 μ_B in $HoCo_2$ and $ErCo_2$. In an attempt to understand the absence of the Co magnetic moments in $RE(Co_{0.667}Ga_{0.333})_2$, the electronic structure was calculated at the LMTO level with no spin polarization or correlation effects included for *RE* = Er. As the observed Co/Ga distribution cannot be handled within LMTO program, the Ga atoms were assigned to the 2*a* sites and Co atoms the 6*h* sites in accordance with the site preferences. The resulting $RE(Co_{0.75}Ga_{0.25})_2$ composition is not too distant from the experimental one. As seen in Fig. 12, the majority of the Co *d* states are below the Fermi level, E_F,

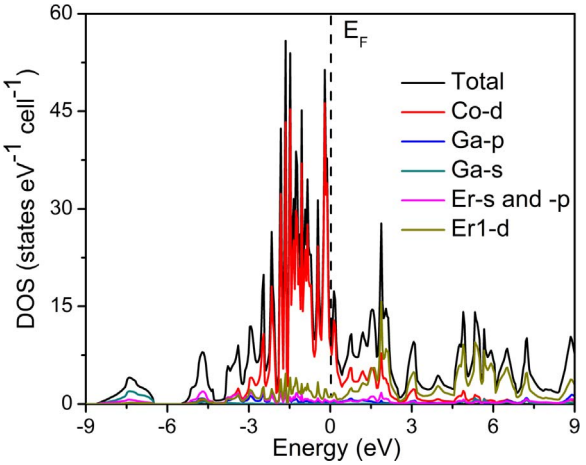

Fig. 12. Density of states (DOS) for $Er(Co_{0.75}Ga_{0.25})_2$.

while the Ga states, particularly the *p* states, and the Er *d* states are well above. Such a distribution is expected due to the much lower energy of the Co *d* orbitals as compared to those of the Ga 4*p* orbitals and Er 5*d* orbitals [25,26]. As well, the Co *d* orbitals are more localized than the Ga 4*p* states. As a result, the Co *d* states are almost fully occupied, E_F falls at a very low density of states (DOS) and the magnetic moment, originating from the *d* electrons, is expected to relatively small or non-existent. Given that the actual Ga concentration is greater and the Co concentration is smaller than calculated, the Co *d* states are likely to be filled to a greater extent than shown in Fig. 12. This situation is consistent with a very small, perhaps zero, experimental Co moment.

4. Conclusions

Variable temperature NPD were collected to clarify the Co/Ga distribution over the 2*a* and 6*h* site and the ground magnetic state of $RE(Co_{0.667}Ga_{0.333})_2$ (*RE* = Ho, and Er). Co and Ga show preferences for the 6*h* and 2*a* sites, respectively. Both materials order ferromagnetically and the Curie temperatures are 31 K and 18.5 K for Ho and Er, respectively, which differ from those inferred from magnetization data, 36 K for Ho and 15 K for Er. At 3.5 K, the Co magnetic moments are close to zero in both materials, and the Er, 6.07(8)μ_B, and Ho, 6.3(1)μ_B, magnetic moments are much smaller than the free ion values, 9 and 10μ_B, respectively, due to crystal field effects. The Er moments are parallel to the *c* axis and there is no change in the magnetic structure as temperature decreases. On the other hand, the Ho moment angle with respect to the *c* axis remains constant between near T_C and 25 K but increases during cooling, reaching 44(1)° at 3.5 K. The MSANS peaks near T_C for $Er(Co_{0.667}Ga_{0.333})_2$ and decreases smoothly with decreasing temperature, a behavior typical for a ferromagnet with no change in magnetic structure. For $Ho(Co_{0.667}Ga_{0.333})_2$ the MSANS increases to a plateau from T_C to 25 K and then increases further during cooling, which tracks the observed change in the Ho moment tilting angle.

Supporting information

Rietveld refinement of NPD data for $Er(Co_{0.667}Ga_{0.333})_2$ and $Ho(Co_{0.667}Ga_{0.333})_2$ at 280 K with λ = 1.327(1) Å and λ = 2.369(1) Å.

Acknowledgements

J.E.G and Y.M. acknowledge the support of the Natural Science and Engineering Research Council of Canada through the Discovery Grant Program. The Canadian Neutron Beam Centre is supported by the Canadian Nuclear Laboratories, Chalk River, Canada.

Appendix A. Supplementary material

Supplementary data associated with this article can be found in the online version at doi:10.1016/j.jssc.2017.09.019.

References

[1] I. Harris, R. Mansey, G. Raynor, J. Less Common Met. 9 (1965) 270–280.
[2] N.H. Duc, T.D. Hien, P.E. Brommer, J.J.M. Franse, J. Magn. Magn. Mater. 104–107 (1992) 1252–1256.
[3] S. Khmelevskyi, P. Mohn, J. Phys. Condens. Matter 12 (2000) 9453–9464.
[4] E. Bash, J. Less-Common Met. 14 (1968) 329–336.
[5] N.K. Singh, K.G. Suresh, A.K. Nigam, S.K. Malik, A.A. Coelho, S. Gama, J. Magn. Magn. Mater. 317 (2007) 68–79.
[6] E. Gratz, A.S. Markosyan, Condens. Matter 13 (2001) 385–413.
[7] V. Franco, J.S. Blázquez, B. Ingale, A. Conde, Annu. Rev. Mater. Res. 42 (2012) 305–342.
[8] N.H. Duc, D.T.K. Anh, J. Magn. Magn. Mater. 242–245 (2002) 873–875.
[9] F. Yuan, J.E. Greedan, Y. Mozharivskyj, J. Magn. Magn. Mater. 441 (2017) 490–496.
[10] V.F. Sears, Neutron News 3 (1992) 29–37.
[11] J. Carvajal-Rodríguez, Physica B 192 (1993) 55–69.
[12] O.K. Andersen, Z. Pawlowska, O. Jepsen, Phys. Rev. B. 34 (1986) 5253–5269.
[13] O. Jepsen, A. Burkhardt, O.K. Andersen, The TB-LMTO-ASA Program, 4.7, Stuttgart, Germany, 1999.
[14] O.K. Andersen, O. Jepsen, Phys. Rev. Lett. 53 (1984) 2571–2574.
[15] O.K. Andersen, O. Jepsen, D. Glotzel, Highlights of condensed matter theory, in: F. Bassani, F. Fumi, M.P. Tosi (Eds.), International Summer School Proc., Elsevier, 1985, p. 59.
[16] O. Jepsen, O.K. Andersen, Phys. B Condens. Matter 97 (1995) 35–47.
[17] L.C. Pauling, The Nature of the Chemical Bond and the Structure of Molecules and Crystals: An Introduction to Modern Structural Chemistry, 3rd ed., Cornell University Press, Ithaca, NY, 1960.
[18] H. Oesterreicher, J. Less-Common Met. 33 (1973) 25–41.
[19] H. Oesterreicher, L.M. Corliss, J.M. Hastings, J. Appl. Phys. 41 (1970) 2326.
[20] M.A. Ruderman, C. Kittel, Phys. Rev. 96 (1954) 99–102.
[21] T. Kasuya, Prog. Theor. Phys. 16 (1956) 45–57.
[22] K. Yosida, Phys. Rev. 106 (1957) 893–898.
[23] J.K. Yakinthos, Conf. Ser. Inst. Phys. 37 (1978) 315–318.
[24] H. Katsuraki, S. Yoshii, J. Phys. Soc. Jpn. 24 (1968) 1171–1172.
[25] J.B. Mann, T.L. Meek, L.C. Allen, J. Am. Chem. Soc. 122 (2000) 2780–2783.
[26] J.B. Mann, T.L. Meek, E.T. Knight, J.F. Capitani, L.C. Allen, J. Am. Chem. Soc. 122 (2000) 5132–5137.